

www.acsami.org Perspective

# **Durable Metal Heteroanionic Photocatalysts**

Kaustav Chatterjee and Sara E. Skrabalak\*



Cite This: ACS Appl. Mater. Interfaces 2021, 13, 36670-36678

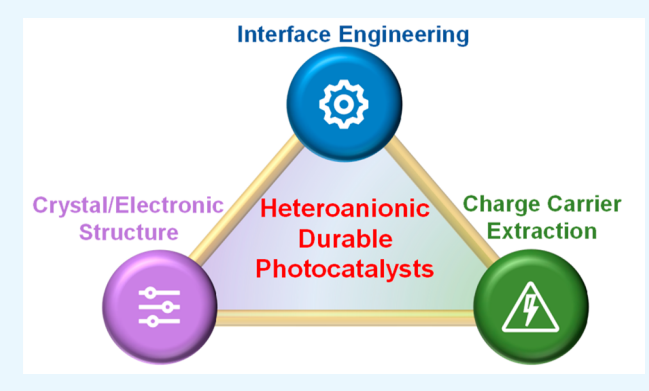


**ACCESS** 

Metrics & More

Article Recommendations

ABSTRACT: Heterogeneous photocatalysis provides a promising strategy to generate renewable fuels by harnessing solar energy. Metal heteroanionic photocatalysts have gained attention for their visible-light absorption; however, they are also plagued by photocorrosion, which limits their long-term use. Such photocorrosion occurs from photooxidation of the less electronegative nonoxide ions, leading to decomposition of the material's lattice. In this Perspective, we highlight emerging strategies to develop durable metal heteroanionic photocatalysts. We devote attention to the approaches taken for model metal oxynitrides, oxysulfides, and oxyhalide photocatalysts to provide a holistic framework. This analysis emphasizes the vital roles that interface engineering, charge carrier extraction, and crystal and electronic structure play in



providing photodurability. We believe that through these approaches, durable and visible-light-absorbing artificial photosynthetic systems can be developed for a sustainable future.

KEYWORDS: photocatalysis, durability, metal heteroanionic, mixed-anion, solar fuels, water splitting, carbon dioxide reduction

# 1. INTRODUCTION

Artificial photosynthetic approaches involving heterogeneous catalysts have been studied for decades to achieve "solar fuels" as renewable chemical feedstocks by water splitting or  $CO_2$  fixation. The Recent efforts show that large-scale photocatalytic water splitting panels have the potential to reach practical industrial-scale use. Thotocatalysts with visible-light absorption, excellent efficiency, and durability are imperative to accomplish this objective. Three basic processes take place on semiconductor photocatalysts. First, photon absorption leads to excitation of electrons (e<sup>-</sup>) from the valence band (VB) to the conduction band (CB), leaving holes (h<sup>+</sup>) in the VB. The second step involves charge separation and migration of excitons (e<sup>-</sup>/h<sup>+</sup> pairs) to the semiconductor surface. The final step involves surface chemical reactions such as the oxygen evolution reaction (OER), hydrogen evolution reaction (HER), and  $CO_2$  reduction reaction ( $CO_2RR$ ).

Traditional photocatalysts are metal oxides containing  $d^0$  or  $d^{10}$  transition metals such as  $TiO_2$ ,  $SrTiO_3$ , or  $ZnO.^{10}$  But because of their large bandgaps, these materials cannot harvest visible light, which comprises much of the solar spectrum reaching Earth's surface. The possibility of having more than one anion has opened directions to develop novel photocatalysts via electronic structure engineering, crystal structure engineering, local coordination geometry, etc. Therefore, metal heteroanionic photocatalysts, such as metal oxynitrides, oxysulfides, and oxyhalides, are emerging as promising materials that exhibit visible-light absorption and provide

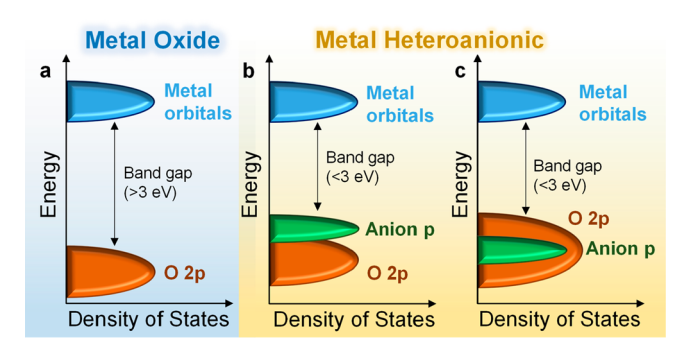
room for VB engineering by judicious manipulation of anions. 11,12

Figure 1 compares the electronic structure of metal oxides and metal heteroanionic photocatalysts. Often, metal oxides of the type MO<sub>x</sub> have large bandgaps (>3 eV), with VBs and CBs composed of O 2p orbitals and metal d orbitals, respectively (Figure 1a). In contrast, metal heteroanionic photocatalysts have smaller bandgaps (<3 eV) due to the lower electronegativity of the nonoxide anions, enabling visible-light absorption. The VB maximum (VBM) of most metal heteroanionic materials of the type MO<sub>x</sub>N<sub>y</sub> (metal oxynitrides),  $M_xO_yS_z$  (metal oxysulfides), and MOX (metal oxyhalides) are composed of the nonoxide p orbitals (N 2p or S 3p or X np) (Figure 1b). This electronic structure can present a challenge as photogenerated h<sup>+</sup> can oxidize nonoxide ions at the VBM in tandem with the desired catalytic oxidation reaction such as OER.13 Figure 1c illustrates that metal heteroanionic photocatalysts of the type Bi<sub>4</sub>MO<sub>8</sub>X or Bi<sub>2</sub>LnO<sub>4</sub>X have a unique electronic structure where the anion p orbitals are buried inside the O 2p orbitals, leading to greater photodurability compared to metal heteroanionic

Received: May 26, 2021 Accepted: July 16, 2021 Published: July 28, 2021







**Figure 1.** Simplified schemes of the electronic structure of (a) metal oxides such as  $MO_x$  and metal heteroanionic photocatalysts such as (b) metal oxynitrides, oxysulfides and oxyhalides of the form  $MO_xN_y$ .  $M_xO_yS_z$ , and MOX and (c) metal oxyhalides of the type  $Bi_4MO_8X$ ,  $Bi_1LnO_4X$ ,  $PbBiO_2X$ , etc.

photocatalysts of the type shown in Figure 1b. In this Perspective, we highlight strategies that have emerged to develop durable metal heteroanionic photocatalysts in tandem with enhanced catalytic efficiency and visible-light absorption. These strategies include surface and interface engineering as well as crystal and electronic structure modifications depending on the material. We note that the examples presented are not comprehensive but were selected as models to illustrate the main conceptual approaches to achieving durable heteroanionic photocatalysts.

## 2. METAL OXYNITRIDES

Metal oxynitrides have VBs composed of nitrogen and oxygen and CBs composed of d<sup>0</sup>- or d<sup>10</sup>-metal orbitals.  $^{14-18}$  As they pose smaller bandgaps relative to corresponding oxides, they are colored materials and absorb visible-light.  $^{19-22}$  TaON, LaTaON<sub>2</sub>, CaTaO<sub>2</sub>N, and BaTaO<sub>2</sub>N are a few examples of photocatalysts having the electronic structure shown in Figure 1b.  $^{23-26}$  The primary cause of loss in the durability of metal oxynitride photocatalysts is the oxidation of the N<sup>3-</sup> ions of the crystal structure by photogenerated h<sup>+</sup> as shown in eq 1:

$$2N^{3-} + 6h^{+} \rightarrow N_{2}$$
 (1)

This reaction occurs as the VBMs consist of N 2p orbitals, and this photooxidation can lead to surface oxide formation. Such modification of the photocatalyst can reduce light absorption and create unfavorable interfaces that limit charge migration

between the bulk and surface material.  $^{9,27-29}$  To curb this photocorrosion process, researchers have developed surface and interface engineering strategies, as discussed herein for TaON and LaMg<sub>x</sub>Ta<sub>1-x</sub>O<sub>1+3x</sub>N<sub>2-3x</sub>, which were selected for emphasis given their promise as widely studied water splitting photocatalysts.  $^{23,30-33}$ 

The synthesis of TaON typically involves heating Ta<sub>2</sub>O<sub>5</sub> under continuous ammonia flow at ~1123 K.34-36 Such a process leads to reduction of Ta<sup>5+</sup> to Ta<sup>4+</sup> or Ta<sup>3+</sup>, which introduces surface anion vacancies to achieve charge balance. The vacancies act as recombination centers of photogenerated charge carriers, thereby reducing activity and durability. To effectively mitigate recombination centers, Maeda et al. prepared a composite of monoclinic zirconium oxide (m-ZrO<sub>2</sub>) and Ta<sub>2</sub>O<sub>5</sub> as a precursor.<sup>37</sup> Ammonolysis of this precursor composite leads to Ta-N-Zr linkages in the m-ZrO<sub>2</sub>/TaON composite produced after nitridation. These Ta-N-Zr linkages provide the Ta species more positive character (close to +5) than unmodified TaON with only Ta-N-Ta linkages. The decrease in anion vacancies led to enhanced proton reduction, but the inherent problem of photodurability (via eq 1 and the electronic structure consistent with Figure 1b) persisted. Maeda et al. further showed that on loading IrO<sub>2</sub> as an OER cocatalyst to the ZrO2/TaON photocatalyst enhanced photodurability was achieved by promoting OER over N<sub>2</sub> evolution.<sup>38</sup> The efficient transfer of h<sup>+</sup> to water from the IrO<sub>2</sub> cocatalyst suppressed photooxidation of TaON.

Another interesting metal oxynitride photocatalyst is LaMg $_x$ Ta $_{1-x}$ O $_{1+3x}$ N $_{2-3x}$  (x=0-0.66). It has the perovskite-type crystal structure shown in Figure 2a and was synthesized from LaTaON $_2$  and LaMg $_{2/3}$ Ta $_{1/3}$ O $_3$ . He absorption of the LaMg $_x$ Ta $_{1-x}$ O $_{1+3x}$ N $_{2-3x}$  solid solutions could be tuned from 525 to 640 nm by modulating x from 0 to 0.66. Pan et al. found the x=0.33 was most active for overall water splitting with RhCrO $_x$  as a suitable HER cocatalyst. However, irradiation ( $\lambda \geq 300$  nm) of RhCrO $_x$ -loaded LaMg $_{0.33}$ Ta $_{0.66}$ O $_2$ N also resulted in continuous N $_2$  evolution (via eq 1) owing to oxidation by photogenerated h<sup>+</sup>. The authors also observed that the rate of the OER increased and then decreased with time, unlike HER. This observation was attributed to the oxygen reduction reaction (ORR) in competition with OER and became dominant in the latter part of the irradiation period.

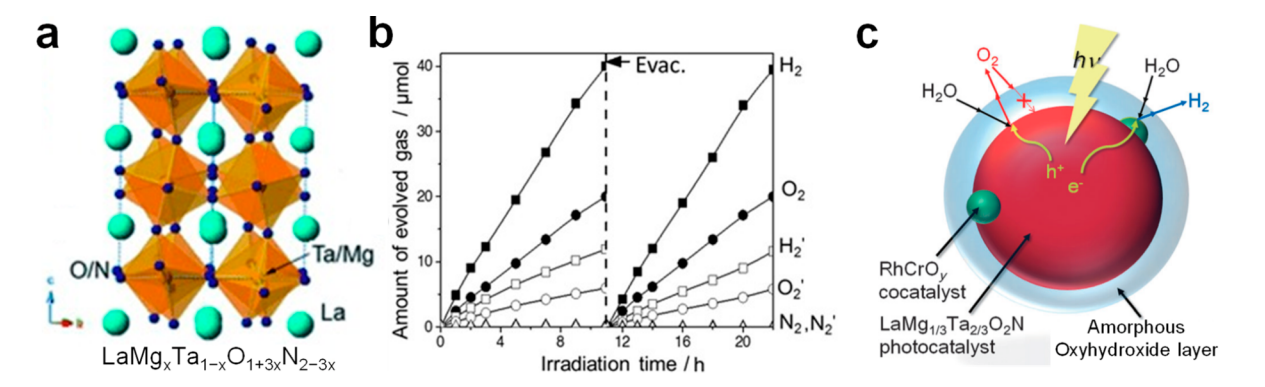


Figure 2. (a) Crystal structure of  $LaMg_xTa_{1-x}O_{1+3x}N_{2-3x}$ . (b) Time course of  $H_2$  and  $O_2$  evolution on  $TiOH/SiOH/RhCrO_x/LaMg_{0.33}Ta_{0.66}O_2N$  under UV/visible irradiation ( $\lambda \geq 300$  nm; filled symbols) and visible-light irradiation alone ( $\lambda \geq 420$  nm; open symbols). (c) Proposed mechanism of charge carrier migration and transfer for water splitting on an amorphous surface-coated photocatalyst. Reprinted with permission from ref 32. Copyright 2015 Wiley–VCH.

Yoshida et al. showed that an Cr oxyhydroxide coating  $(CrO_{(1.5-m)}(OH)_{2m} \cdot xH_2O)$  layer, denoted as MOH herein on top of the photocatalyst helped to reduce the ORR. 41 Likewise, Pan et al. loaded a thin coating of amorphous titanium oxyhydroxide (TiOH) on RhCrO<sub>x</sub>/LaMg<sub>0.33</sub>Ta<sub>0.66</sub>O<sub>2</sub>N, which prevented both N2 evolution and the ORR, thereby leading to enhanced durability and activity. 32,33 Interestingly, Pan et al. observed N<sub>2</sub> evolution upon coating Si oxyhydroxide (SiOH) on RhCrOx/LaMg0.33Ta0.66O2N. Combining SiOH with TiOH, however, led to greater photocatalytic activity and durability over 22 h than coating alone, as shown in Figure 2b. 32 The authors speculated that the reduced photocorrosion resulted from the facile transfer of photogenerated h+ to the amorphous layer. In effect, this modification prevented the accumulation of h<sup>+</sup> on the oxynitride surface to carry out eq 1. This prevention led the OER to take place at the interface between the oxynitride and the amorphous oxyhydroxide layer or in the amorphous oxyhydroxide layer, as shown in Figure

As these studies have shown, surface and interface modification can enhance the durability of metal oxynitride photocatalysts. These modifications provide durability by managing h+ extraction and are essential to realizing metal oxynitrides as visible-light absorbing photocatalysts. Still, future innovations that improve durability of metal oxynitrides may be possible by considering how durability is engineered in other heteroanionic materials.

#### 3. METAL OXYSULFIDES

Metal oxysulfides are a class of heteroanionic photocatalysts with VBs composed of sulfur and oxygen orbitals, and the CBs are occupied by do- or do-metal ion orbitals such as in Ln<sub>2</sub>Ti<sub>2</sub>S<sub>2</sub>O<sub>5</sub> (Ln = Nd, Sm, Gd, Tb, Dy, Ho, Er, and Y) and SrZn<sub>2</sub>S<sub>2</sub>O. 42-45 Metal oxysulfides are mostly synthesized from oxide precursors, with sulfur being introduced from sulfur powder or metal sulfides. 43,46,45 However, synthesizing oxysulfide photocatalysts with tunable bandgaps through stoichiometric control is difficult given the larger atomic size of sulfur than oxygen. Still, when compared to metal sulfides such as CdS or ZnS, metal oxysulfides are less prone to self-oxidation by photogenerated h<sup>+</sup>, as shown by eq 2:

$$2S^{2-} + 2h^{+} \to S_{2}^{2-} \tag{2}$$

This tendency can be attributed to the hybridization of the S 3p-O 2p orbitals in the VBM, unlike only S 3p orbitals for metal sulfides. Moreover, efficient extraction of photogenerated h+ can enhance the durability of metal oxysulfides. Strategies that achieve this objective will be outlined for Y2Ti2O5S2 as a model system, which was selected for emphasis on account of its nearly ideal band gap (1.9 eV) for overall water splitting.

Employing appropriate OER cocatalysts on oxysulfide photocatalysts were found to be effective in extracting h+ from oxysulfides.<sup>43</sup> For example, Wang et al. demonstrated Y<sub>2</sub>Ti<sub>2</sub>O<sub>5</sub>S<sub>2</sub> for overall water splitting with remarkable photostability. 47 The material was prepared by solid-state synthesis from stoichiometric amounts of Y2O3, Y2S3, TiO2, and sulfur. Using IrO<sub>2</sub> as an OER cocatalyst and Rh@Cr<sub>2</sub>O<sub>3</sub> (core@shell) nanoparticles as a HER cocatalyst, overall water splitting was achieved with the desired ratio of  $H_2$  to  $O_2$  of 2:1. Notably, Wang et al. reported that the order of cocatalyst loading affects photocatalytic activity. Loading the OER cocatalyst before the HER cocatalyst led to greater activity by 30% compared to the

reverse. Such an enhancement arose from the preferential attachment of the HER cocatalyst at the reduction sites by photodeposition. Also, it prevents the deposition of IrO2 on top of Cr<sub>2</sub>O<sub>3</sub>/Rh. The observed phenomenon suggests that the cocatalysts should be loaded onto different regions of photocatalyst to enhance the efficacy effectively. In addition to rapid h<sup>+</sup> extraction by the IrO<sub>2</sub> cocatalysts, the authors hypothesized that the durability arose from the material's electronic structure. A band structure calculation of Y<sub>2</sub>Ti<sub>2</sub>O<sub>5</sub>S<sub>2</sub> revealed significant hybridization between the orbitals of S and O near the VBM (similar to Figure 1b). This phenomenon reduces the oxidation of sulfur ions from lattice (eq 2), thereby enhancing durability.

Metal oxysulfide photocatalysts are less studied compared to other metal heteroanionic compounds. The key factors to improve photostability include developing appropriate cocatalysts that can extract h+/e- from photocatalyst and strong hybridization between sulfur and oxygen orbitals near VBM. The latter factor, in which the electronic structure of material contributes directly toward its durability, will also be encountered in the next section discussing metal oxyhalides.

#### 4. METAL OXYHALIDES

Metal oxyhalides are another class of metal heteroanionic photocatalysts. The VBs of oxyhalides are composed of O 2p orbitals and X np orbitals (n = 3, 4, and 5 for X = Cl, Br, and I).48-50 The aforesaid electronic structure enables the customization of the bandgap in oxyhalides by engineering the halide (Cl, Br, and I) identity. We have focused on metal oxyhalides with  $d^{10}$  metal cations (such as  $Bi^{3+}$ ) given their suitability for photocatalysis.

Metal oxyhalides of the type BiOX (X = Cl, Br, I) have gained significant interest owing to their ability to change the bandgap based on the halide identity. 54,55 With the increase in size of the halogen ion, the polarizability increases from Cl to I, which is associated with greater visible light absorption.<sup>50</sup> These materials consist of  $[Bi_2O_2]^{+2}$  layers between double slabs of X<sup>-</sup> atoms. The stacking of oppositely charged layers leads to an internal electric field (IEF) within the crystal structure. 57-61 The built-up IEF facilitates separation of e<sup>-</sup> and h<sup>+</sup> when illuminated by photons of appropriate energy. 49,50 Density functional theory (DFT) calculations on BiOX photocatalysts illustrate that the VB consists primarily of hybrid O 2p and X np orbitals, whereas the CB consists of Bi 6p orbitals. Even though certain BiOX materials can absorb visible light, they often undergo photooxidation by the photogenerated h<sup>+</sup> according to the following eq 3:

$$2X^- + 2h^+ \to X_2 \tag{3}$$

Such photooxidation will be more severe for those metal oxyhalides with a greater density of X np orbitals near the VBM in accordance with Figure 1b. 51,56 Such a phenomenon necessities the development of metal oxyhalides with stability against photocorrosion.

Recently, metal oxyhalides of the type Bi<sub>4</sub>MO<sub>8</sub>X (M = Ta, Nb; X = Cl, Br) have shown potential as durable photocatalysts with visible-light irradiation. 62-66 Bi<sub>4</sub>MO<sub>8</sub>X materials are layered Sillen-Aurivillius perovskites whose structure is composed of Sillen blocks (alternating [Bi<sub>2</sub>O<sub>2</sub>]<sup>+2</sup>, X<sup>-</sup> slabs) and Aurivillius blocks (alternating  $[Bi_2O_2]^{+2}[MO_4]^{-3}$  slabs). Density of states (DOS) calculated for Bi<sub>4</sub>MO<sub>8</sub>X indicate that the VBM are composed of Bi 6s and O 2p orbitals while the nonoxide halogen orbitals contribute to lower energy states

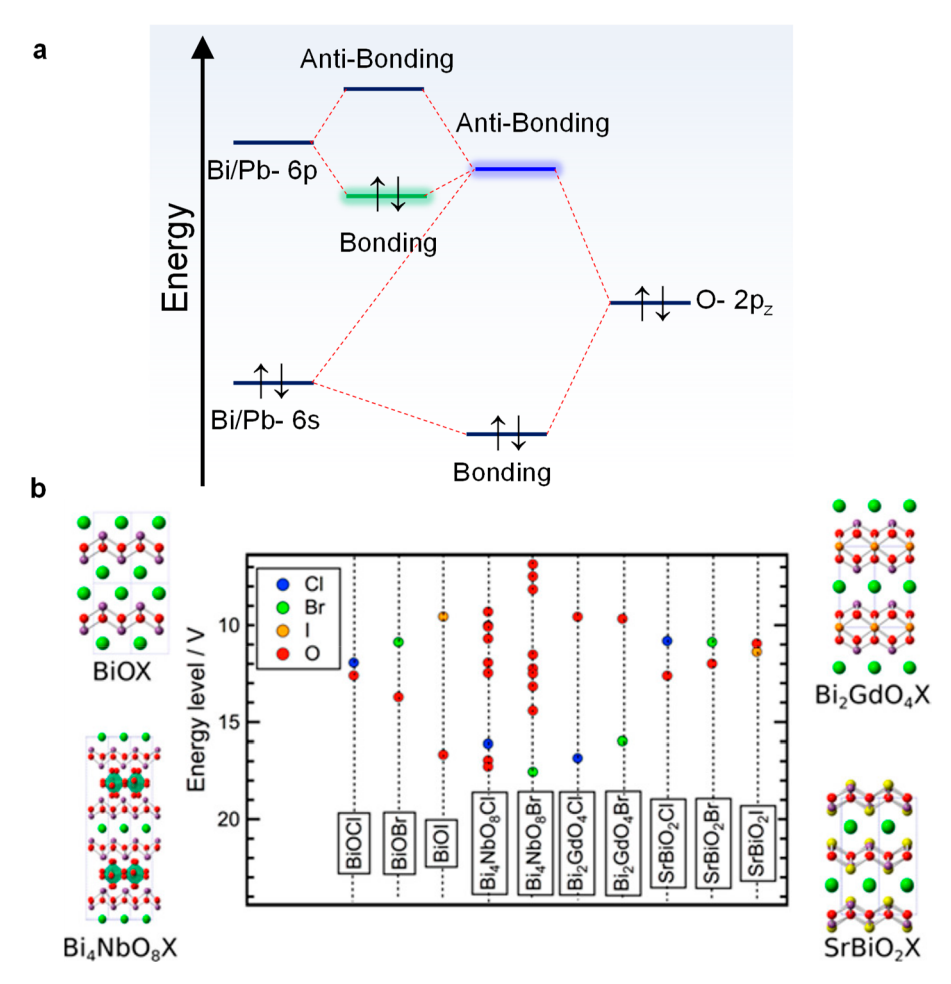


Figure 3. (a) Schematic interaction between Bi/Pb 6s, Bi/Pb 6p, and O 2p orbitals based on the revised lone pair (RLP) model. (b) Ionic energy levels for each anionic site in BiOX,  $Bi_4NbO_8X$ ,  $Bi_2GdO_4X$ , and  $SrBiO_2X$  calculated by the sum of the Madelung potential and electron affinity. The red, blue, green, and orange symbols represent oxygen, chlorine, bromine, and iodine anions, respectively. Reprinted with permission from ref 71. Copyright 2017 American Chemical Society.

in the valence band (similar to Figure 1c rather than Figure 1b).<sup>68</sup> Importantly, the observed electronic structure preserves the visible-light-absorbing capability of these oxyhalide materials. The unique electronic structure leads to enhanced photodurability by suppression of eq 3.

Such a distinctive electronic structure is explained by the revised lone pair (RLP) model developed by Watson and coworkers.<sup>69,70</sup> Examination of the partial DOS of Bi<sub>4</sub>MO<sub>8</sub>X found the contribution of the Bi 6p orbitals in addition to Bi 6s and O 2p orbitals near the VB.71,72 Strong hybridization between stereochemically active Bi3+ 6s2 lone pairs and O 2p orbitals occurs to form a (Bi 6s + O 2p) bonding orbital and high energy (Bi 6s + O 2p)\* antibonding orbital shown in Figure 3a. Because of crystal distortion, the high-energy (Bi 6s + O 2p)\* antibonding orbital interacts with the vacant Bi 6p orbital. The interaction of the antibonding orbital and the Bi 6p orbital results in asymmetric electron density over the Bi<sup>3+</sup> lone pair, leading to stabilization of the (Bi 6s + O 2p)\* antibonding orbital. Aforementioned stabilization elevates the VBM in Bi₄MO<sub>8</sub>X, with dispersive O 2p orbitals in the VB. A similar electronic structure has been reported for PbBiO<sub>2</sub>X (X = Cl, Br, I), involving Pb<sup>2+</sup> 6s<sup>2</sup> lone pairs and O 2p orbitals, as shown in Figure 3a. 73 Kunioku et al. estimated the degree of such hybridization in Bi<sub>4</sub>MO<sub>8</sub>X systems around 0.19-0.20 compared to 0.15 in BiOX systems. 72 Thus, the question lies in

why such dispersive O 2p states were not observed in BiOX compared to  $Bi_4MO_8X$  photocatalyst systems.

To investigate the question, Kato et al. used a local theoretical calculation approach composed of the electrostatic potential created at the selected crystallographic site by neighboring ions or Madelung site potential. 71 Figure 3b shows the sum of the Madelung site potentials and the electron affinities along with the crystal structures of BiOX and Bi<sub>4</sub>NbO<sub>8</sub>X. In Bi<sub>4</sub>NbO<sub>8</sub>X, the energy of most oxygen sites was higher than the halogen sites, which is in stark contrast to the BiOX case. Although the eight oxygen sites of Bi<sub>4</sub>NbO<sub>8</sub>X have different energies, on a closer look, the authors reported the O sites from the fluorite-like [Bi<sub>2</sub>O<sub>2</sub>] slabs were more destabilized than the [NbO<sub>4</sub>] slab. Thus, the observed unique band structure of Bi<sub>4</sub>NbO<sub>8</sub>X was caused by electrostatic destabilization of oxide anions and stabilization of X ions. Notably, Kato et al. could not unveil the origin of the difference in the electronic structures of BiOX and Bi<sub>4</sub>NbO<sub>9</sub>X. The reason being the structural complexity of Bi<sub>4</sub>NbO<sub>8</sub>X (heavy distortion of NbO<sub>6</sub>) vs undistorted BiOX. The authors further carried out similar Madelung site analysis for Bi<sub>2</sub>GdO<sub>4</sub>X and SrBiO<sub>2</sub>X systems (Figure 3b) with less distorted lattices, which offer detailed comparison to BiOX.<sup>71</sup>

All these theoretical foundations were developed due to the exceptional photocatalytic durability observed by Abe and co-

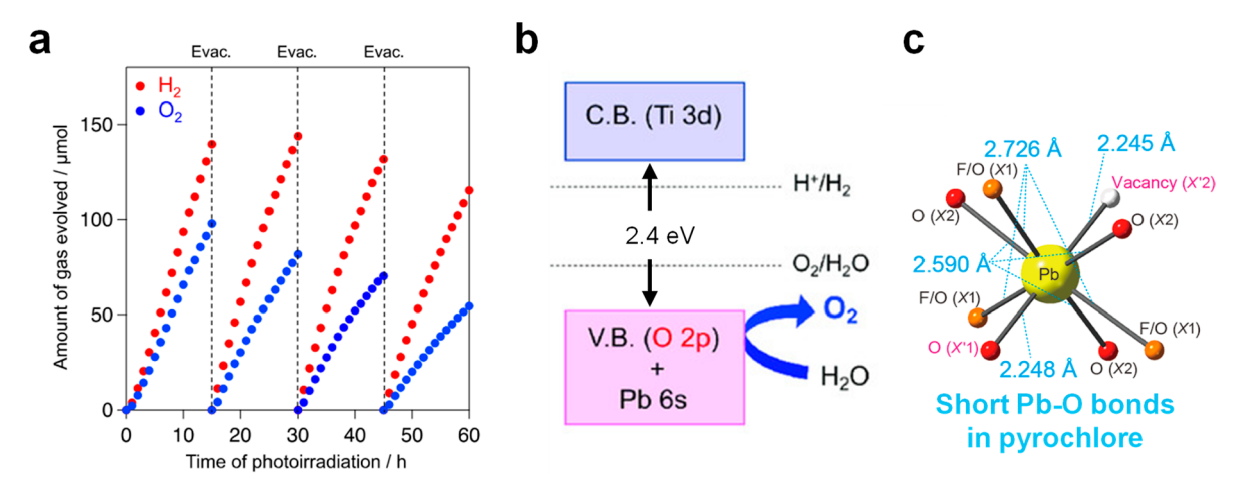


Figure 4. (a) Time course of Z-scheme water splitting of  $Bi_4NbO_8Cl$  coupled with  $Ru/SrTiO_3$ :Rh photocatalyst via an  $Fe^{3+}/Fe^{2+}$  redox mediator under visible-light ( $\lambda > 400$  nm) irradiation. Reprinted with permission from ref 63. Copyright 2016 American Chemical Society. (b) Schematic band structure illustration of  $Pb_2Ti_2O_{5,4}F_{1,2}$ . Adapted with permission from ref 76. Copyright 2019, American Chemical Society. (c) Coordination geometry around Pb and O depicting the shorted Pb—O bond distances in the pyrochlore crystal structure. Adapted with permission from ref 76. Copyright 2018 American Chemical Society.

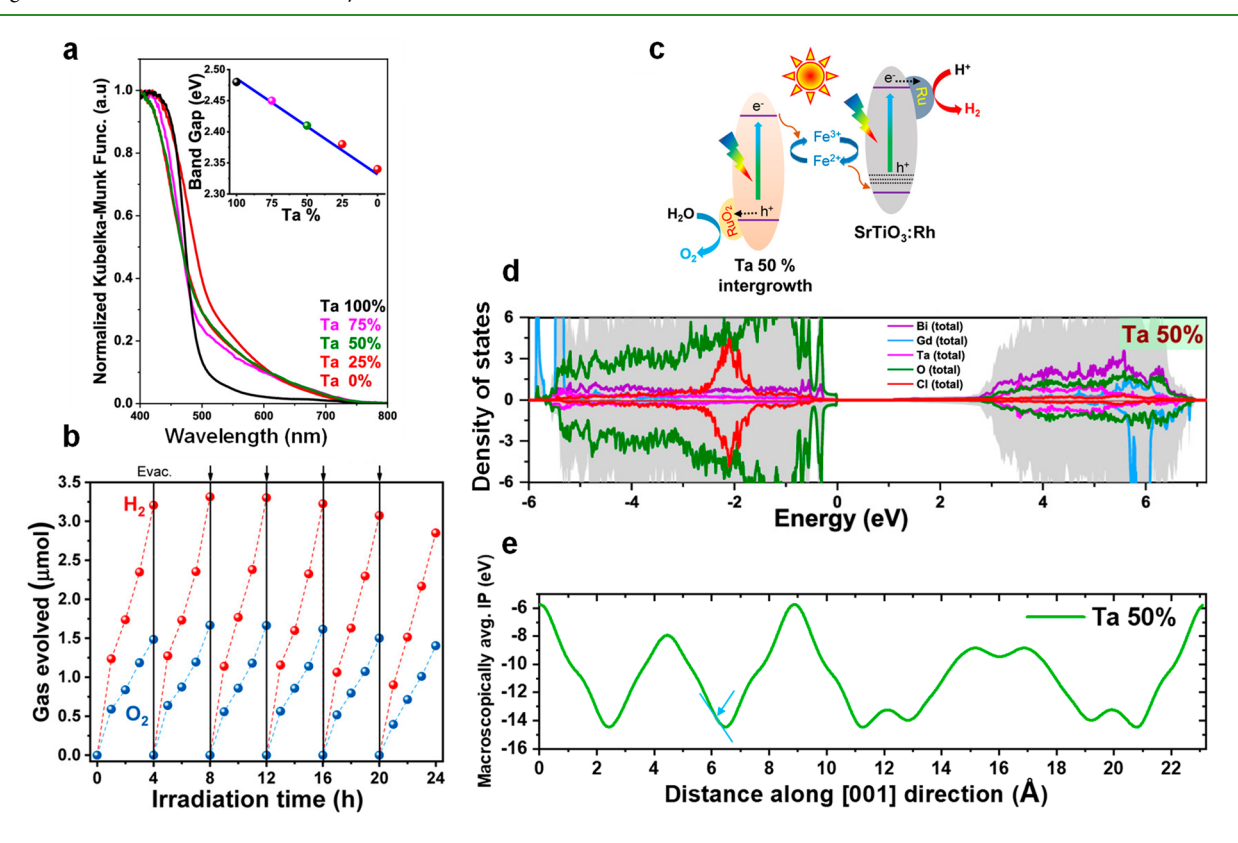


Figure 5. (a) UV/visible diffuse reflectance spectra of the intergrowths; the inset indicates the change in bandgap as a function of Ta X %. (b) Time course of Z-scheme overall water splitting on  $RuO_2$ -loaded Ta 50% and  $Ru/SrTiO_3$ :Rh using a  $Fe^{3+}/Fe^{2+}$  redox mediator using a 300 W Xe lamp with an AM 1.5G filter. (c) Proposed mechanism of electron transfer in the two photocatalyst systems in the Z-scheme overall water splitting using the redox mediator. (d) Total DOS plots of the Ta 50% intergrowth sample. (e) Macroscopically averaged local internal potential (IP) along the [001] direction for the Ta 50% sample, the magnitude of electric field  $\propto$  slope of the curve (arrowed). Reprinted with permission from ref 79. Copyright 2021 American Chemical Society.

workers in Bi<sub>4</sub>NbO<sub>8</sub>X (X= Cl, Br).<sup>63,74</sup> Bi<sub>4</sub>NbO<sub>8</sub>Cl exhibited continuous photocatalytic activity for the OER in the presence of sacrificial reagents with an apparent quantum efficiency (AQE) of 0.4% at 420 nm.<sup>63</sup> Interestingly, the authors reported no notable change of crystal structure after photoirradiation. Further, the amount of Cl<sup>-</sup> ions was almost constant, demonstrating stability against self-oxidation by

photogenerated  $h^+.$  On employing a Z-scheme for overall water splitting, a continuous evolution of  $H_2$  and  $O_2$  at appropriate stoichiometry was observed for 60 h, as shown in Figure 4a.  $^{63}$  Similar photodurability was also achieved with  $Bi_4TaO_8X\ (X=Cl,\ Br)$  by Tao et al. using a Z-scheme.  $^{65,75}$  Also, they achieved an AQE of 22.3% at 420 nm for OER with  $RuO_2\text{-loaded}\ Bi_4TaO_8Br.$ 

Recently Kuriki et al. developed a Pb-based oxyfluoride, Pb<sub>2</sub>Ti<sub>2</sub>O<sub>5,4</sub>F<sub>1,2</sub>, as a durable narrow bandgap (2.4 eV) photocatalyst both for the HER and CO2RR under visiblelight irradiation.<sup>76</sup> Interestingly, the durability of this system stems from the fact that the VBM consists of O 2p and Pb 6s orbitals, as elucidated by DFT calculations shown in Figure 4b. 76-78 The crystal structure of Pb2Ti2O5.4F1.2 is an oxygendeficient A<sub>2</sub>B<sub>2</sub>X<sub>6</sub>X'<sub>0.5</sub> pyrochlore structure. Pb<sub>2</sub>Ti<sub>2</sub>O<sub>5.4</sub>F<sub>1.2</sub> is composed of shorter Pb—O bond distances than conventional A—O bonds shown in Figure 4c due to fluorine substitution. <sup>76</sup> The shorter bond distances cause strong hybridization of the Pb 6s and O 2p orbitals, as shown in Figure 3a. This strong interaction causes an upward shift in the VB, thereby lowering the bandgap of Pb<sub>2</sub>Ti<sub>2</sub>O<sub>5.4</sub>F<sub>1.2</sub> (2.4 eV) vs. PbTiO<sub>3</sub> (2.8 eV) which has higher Pb-O bond distances. The photoelectrocatalytic OER was performed by cocatalyst modified Pb<sub>2</sub>Ti<sub>2</sub>O<sub>54</sub>F<sub>1,2</sub> photoanode under simulated sunlight irradiation (AM1.5G, 100 mW cm<sup>-2</sup>) in the presence of an applied potential of +0.90 V vs RHE with faradaic efficiency of 93%.<sup>78</sup> Thus, signifying the effective utilization of the photogenerated h<sup>+</sup> during light irradiation.

Recently, our group reported Bi<sub>4</sub>TaO<sub>8</sub>Cl-Bi<sub>2</sub>GdO<sub>4</sub>Cl intergrowths for visible-light-responsive water splitting. 79,80 An intergrowth is a compound crystal phase with elemental homogeneity at the nanoscale, which differentiates it from composite materials where such homogeneity is not present. The Ta:Gd molar ratio was varied to understand the effect of intergrowth composition on the electronic structure. We observed, moving from Ta 100% to Ta 0%, the bandgap changes from 2.48 to 2.34 eV, as shown in Figure 5a. Photocatalytic OER activity was highest for Ta 50% among the intergrowths, and RuO2 loaded Ta 50% demonstrated AQE of 7.6% (400-500 nm). Overall water splitting was achieved using cocatalyst loaded Ta 50% intergrowth with Ru/ SrTiO3:Rh as the HER catalyst under simulated solar illumination for 24 h with minimal loss in durability shown in Figure 5b. The schematic of the electron transfer process in the overall water splitting reaction is shown in Figure 5c. DOS calculations on Ta 50% elucidated the presence of O 2p orbitals predominantly over the VBM rather than Cl 3p (Figure 5d) orbitals. The observed electronic structure can be explained by the hybridization of Bi 6s and O 2p orbitals near the VBM based on the RLP model. Thus, it accounts for the high durability of these new mixed metal oxychloride materials. Notably, modulation of IEFs via manipulating the perovskite slabs (Ta/Gd) led to the enhanced separation of charge carriers of the Ta 50% intergrowth, shown in Figure 5e. These observations support our hypothesis that the formation of intergrowth materials can enhance photocatalytic activity with the preservation of durability.

The strategy to obtain durable photocatalytic metal oxyhalides has been developing semiconductors whose VB are dominated by dispersive O 2p orbitals such as *Sillen-Aurivillius* perovskites. Related layered structures such as Bi<sub>2</sub>AO<sub>4</sub>X (A = Y, La, Gd, Bi), PbBiO<sub>2</sub>X and SrBiO<sub>2</sub>X (X = Cl, Br) have also shown similar VB structures.<sup>73,81</sup> Additionally, recent research efforts involving novel synthetic methods, modulation of surface carriers, and developing new oxyhalides by layer insertion have gained attraction on these *Sillen-Aurivillius* perovskites.<sup>82–84</sup>

## 5. CONCLUSION AND FUTURE OUTLOOK

Recent advances in interface engineering and cocatalyst selection are providing durable photocatalytic materials based on metal heteroanionic compositions. Additionally, the engineering of the interaction between post-transition metal s orbitals such as Bi/Pb 6s and O 2p orbitals has opened new directions to obtain photocatalysts with remarkable photostability based on their electronic structure. These approaches do not require surface modification by coating techniques to suppress photocorrosion and are attractive in terms of exposing appropriate surface structures to undergo efficient catalysis. Further, layered materials facilitate IEF modulation by intergrowth formation, with preservation of durability. However, challenges in synthetic methodologies for developing tailor-made metal heteroanionic materials still exist, such as the formation of anion defects due to different volatility of the ions. New strategies are emerging to address these issues via flux-based or polymerized complex techniques. 20,82,74,79 The field is still growing to deliver next-generation artificial photosynthetic systems with state-of-the-art optoelectronic properties to address the global energy demand.

## AUTHOR INFORMATION

### **Corresponding Author**

Sara E. Skrabalak — Department of Chemistry, Indiana University, Bloomington, Indiana 47405, United States; orcid.org/0000-0002-1873-100X; Email: sskrabal@indiana.edu

#### **Author**

Kaustav Chatterjee — Department of Chemistry, Indiana University, Bloomington, Indiana 47405, United States; orcid.org/0000-0003-3527-9796

Complete contact information is available at: https://pubs.acs.org/10.1021/acsami.1c09774

## **Author Contributions**

The manuscript was written through contributions of all authors. All authors have given approval to the final version of the manuscript.

## **Funding**

This work was supported by Indiana University and US NSF DMR-2113536.

#### Note

The authors declare no competing financial interest.

# ACKNOWLEDGMENTS

The authors thank all research scholars and collaborators who have supported this project and contributed to the cited manuscripts.

## REFERENCES

- (1) Kudo, A.; Miseki, Y. Heterogeneous Photocatalyst Materials for Water Splitting. *Chem. Soc. Rev.* **2009**, *38*, 253–278.
- (2) Osterloh, F. E. Inorganic Nanostructures for Photoelectrochemical and Photocatalytic Water Splitting. *Chem. Soc. Rev.* **2013**, *42*, 2294–2320.
- (3) White, J. L.; Baruch, M. F.; Pander, J. E.; Hu, Y.; Fortmeyer, I. C.; Park, J. E.; Zhang, T.; Liao, K.; Gu, J.; Yan, Y.; Shaw, T. W.; Abelev, E.; Bocarsly, A. B. Light-Driven Heterogeneous Reduction of Carbon Dioxide: Photocatalysts and Photoelectrodes. *Chem. Rev.* **2015**, *115*, 12888–12935.

- (4) Walter, M. G.; Warren, E. L.; McKone, J. R.; Boettcher, S. W.; Mi, Q.; Santori, E. A.; Lewis, N. S. Solar Water Splitting Cells. *Chem. Rev.* **2010**, *110*, 6446–6473.
- (5) Hisatomi, T.; Domen, K. Reaction Systems for Solar Hydrogen Production via Water Splitting with Particulate Semiconductor Photocatalysts. *Nat. Catal.* **2019**, *2*, 387–399.
- (6) Goto, Y.; Hisatomi, T.; Wang, Q.; Higashi, T.; Ishikiriyama, K.; Maeda, T.; Sakata, Y.; Okunaka, S.; Tokudome, H.; Katayama, M.; Akiyama, S.; Nishiyama, H.; Inoue, Y.; Takewaki, T.; Setoyama, T.; Minegishi, T.; Takata, T.; Yamada, T.; Domen, K. A Particulate Photocatalyst Water-Splitting Panel for Large-Scale Solar Hydrogen Generation. *Joule* **2018**, *2*, 509–520.
- (7) Liu, G.; Sheng, Y.; Ager, J. W.; Kraft, M.; Xu, R. Research Advances towards Large-Scale Solar Hydrogen Production from Water. *EnergyChem.* **2019**, *1*, 100014.
- (8) Abe, R. Development of a New System for Photocatalytic Water Splitting into  $H_2$  and  $O_2$  under Visible Light Irradiation. *Bull. Chem. Soc. Jpn.* **2011**, *84*, 1000–1030.
- (9) Wang, Q.; Domen, K. Particulate Photocatalysts for Light-Driven Water Splitting: Mechanisms, Challenges, and Design Strategies. *Chem. Rev.* **2020**, *120*, 919–985.
- (10) Maeda, K. Photocatalytic Water Splitting Using Semiconductor Particles: History and Recent Developments. *J. Photochem. Photobiol.,* C **2011**, *12*, 237–268.
- (11) Kageyama, H.; Hayashi, K.; Maeda, K.; Attfield, J. P.; Hiroi, Z.; Rondinelli, J. M.; Poeppelmeier, K. R. Expanding Frontiers in Materials Chemistry and Physics with Multiple Anions. *Nat. Commun.* **2018**, *9*, 772.
- (12) Cui, J.; Li, C.; Zhang, F. Development of Mixed-Anion Photocatalysts with Wide Visible-Light Absorption Bands for Solar Water Splitting. *ChemSusChem* **2019**, *12*, 1872–1888.
- (13) Miyoshi, A.; Maeda, K. Recent Progress in Mixed-Anion Materials for Solar Fuel Production. Sol. RRL 2021, 5, 2000521.
- (14) Maeda, K.; Domen, K. Oxynitride Materials for Solar Water Splitting. MRS Bull. 2011, 36, 25-31.
- (15) Fuertes, A. Metal Oxynitrides as Emerging Materials with Photocatalytic and Electronic Properties. *Mater. Horiz.* **2015**, *2*, 453–461.
- (16) Abeysinghe, D.; Skrabalak, S. E. Toward Shape-Controlled Metal Oxynitride and Nitride Particles for Solar Energy Applications. *ACS Energy Lett.* **2018**, *3*, 1331–1344.
- (17) Balaz, S.; Porter, S. H.; Woodward, P. M.; Brillson, L. J. Electronic Structure of Tantalum Oxynitride Perovskite Photocatalysts. *Chem. Mater.* **2013**, *25*, 3337–3343.
- (18) Chen, D. P.; Skrabalak, S. E. Synthesis of  $(Ga_{1-x}Zn_x)(N_{1-x}O_x)$  with Enhanced Visible-Light Absorption and Reduced Defects by Suppressing Zn Volatilization. *Inorg. Chem.* **2016**, *55*, 3822–3828.
- (19) Chen, D. P.; Neuefeind, J. C.; Koczkur, K. M.; Bish, D. L.; Skrabalak, S. E. Role of Short-Range Chemical Ordering in  $(GaN)_{1-x}(ZnO)_x$  for Photodriven Oxygen Evolution. *Chem. Mater.* **2017**, 29, 6525–6535.
- (20) Fu, J.; Skrabalak, S. E. Enhanced Photoactivity from Single-Crystalline SrTaO<sub>2</sub>N Nanoplates Synthesized by Topotactic Nitridation. *Angew. Chem., Int. Ed.* **2017**, *56*, 14169–14173.
- (21) Rugen, E. E.; Koczkur, K. M.; Skrabalak, S. E. Facile Synthesis of Porous La–Ti–O and LaTiO<sub>2</sub>N Microspheres. *Dalton Trans.* **2017**, *46*, 10727–10733.
- (22) Chen, D. P.; Losovyj, Y.; Skrabalak, S. E. N-Type Doping of Visible-Light-Absorbing  $(GaN)_{1-x}(ZnO)_x$  with Aliovalent Sn/Si Substitutions. *J. Phys. Chem. C* **2018**, *122*, 13250–13258.
- (23) Hitoki, G.; Takata, T.; Kondo, J. N.; Hara, M.; Kobayashi, H.; Domen, K. An Oxynitride, TaON, as an Efficient Water Oxidation Photocatalyst under Visible Light Irradiation ( $\lambda \leq 500$  nm). *Chem. Commun.* **2002**, 1698–1699.
- (24) Ueda, K.; Kato, H.; Kobayashi, M.; Hara, M.; Kakihana, M. Control of Valence Band Potential and Photocatalytic Properties of Na<sub>x</sub>La<sub>1-x</sub>TaO<sub>1+2x</sub>N<sub>2-2x</sub> Oxynitride Solid Solutions. *J. Mater. Chem. A* **2013**, *1*, 3667–3674.

- (25) Xu, J.; Pan, C.; Takata, T.; Domen, K. Photocatalytic Overall Water Splitting on the Perovskite-Type Transition Metal Oxynitride  $CaTaO_2N$  under Visible Light Irradiation. *Chem. Commun.* **2015**, *51*, 7191–7194
- (26) Higashi, M.; Domen, K.; Abe, R. Fabrication of an Efficient  $BaTaO_2N$  Photoanode Harvesting a Wide Range of Visible Light for Water Splitting. *J. Am. Chem. Soc.* **2013**, *135*, 10238–10241.
- (27) Nakamura, R.; Tanaka, T.; Nakato, Y. Oxygen Photoevolution on a Tantalum Oxynitride Photocatalyst under Visible-Light Irradiation: How Does Water Photooxidation Proceed on a Metal—Oxynitride Surface? J. Phys. Chem. B 2005, 109, 8920—8927.
- (28) Weng, B.; Qi, M.-Y.; Han, C.; Tang, Z.-R.; Xu, Y.-J. Photocorrosion Inhibition of Semiconductor-Based Photocatalysts: Basic Principle, Current Development, and Future Perspective. *ACS Catal.* **2019**, *9*, 4642–4687.
- (29) Chen, S.; Huang, D.; Xu, P.; Xue, W.; Lei, L.; Cheng, M.; Wang, R.; Liu, X.; Deng, R. Semiconductor-Based Photocatalysts for Photocatalytic and Photoelectrochemical Water Splitting: Will We Stop with Photocorrosion? *J. Mater. Chem. A* **2020**, *8*, 2286–2322.
- (30) Abe, R.; Higashi, M.; Domen, K. Facile Fabrication of an Efficient Oxynitride TaON Photoanode for Overall Water Splitting into H<sub>2</sub> and O<sub>2</sub> under Visible Light Irradiation. *J. Am. Chem. Soc.* **2010**, *1*32, 11828–11829.
- (31) Higashi, M.; Domen, K.; Abe, R. Highly Stable Water Splitting on Oxynitride TaON Photoanode System under Visible Light Irradiation. *J. Am. Chem. Soc.* **2012**, *134*, 6968–6971.
- (32) Pan, C.; Takata, T.; Nakabayashi, M.; Matsumoto, T.; Shibata, N.; Ikuhara, Y.; Domen, K. A Complex Perovskite-Type Oxynitride: The First Photocatalyst for Water Splitting Operable at up to 600 nm. *Angew. Chem., Int. Ed.* **2015**, *54*, 2955–2959.
- (33) Pan, C.; Takata, T.; Domen, K. Overall Water Splitting on the Transition-Metal Oxynitride Photocatalyst  $LaMg_{1/3}Ta_{2/3}O_2N$  over a Large Portion of the Visible-Light Spectrum. *Chem. Eur. J.* **2016**, 22, 1854–1862.
- (34) Marchand, R.; Laurent, Y.; Guyader, J.; L'Haridon, P.; Verdier, P. Nitrides and Oxynitrides: Preparation, Crystal Chemistry and Properties. *J. Eur. Ceram. Soc.* **1991**, *8*, 197–213.
- (35) de Respinis, M.; Fravventura, M.; Abdi, F. F.; Schreuders, H.; Savenije, T. J.; Smith, W. A.; Dam, B.; van de Krol, R. Oxynitrogenography: Controlled Synthesis of Single-Phase Tantalum Oxynitride Photoabsorbers. *Chem. Mater.* 2015, 27, 7091–7099.
- (36) Matizamhuka, W. R.; Sigalas, I.; Herrmann, M. Synthesis, Sintering and Characterisation of TaON Materials. *Ceram. Int.* **2008**, 34, 1481–1486.
- (37) Maeda, K.; Terashima, H.; Kase, K.; Higashi, M.; Tabata, M.; Domen, K. Surface Modification of TaON with Monoclinic ZrO<sub>2</sub> to Produce a Composite Photocatalyst with Enhanced Hydrogen Evolution Activity under Visible Light. *Bull. Chem. Soc. Jpn.* **2008**, *81*, 927–937.
- (38) Maeda, K.; Lu, D.; Domen, K. Direct Water Splitting into Hydrogen and Oxygen under Visible Light by Using Modified TaON Photocatalysts with d<sup>0</sup> Electronic Configuration. *Chem. Eur. J.* **2013**, 19, 4986–4991.
- (39) Kim, Y.-I.; Woodward, P. M. Syntheses and Characterizations of Complex Perovskite Oxynitrides LaMg $_{1/3}$ Ta $_{2/3}$ O $_2$ N, LaMg $_{1/2}$ Ta $_{1/2}$ O $_{5/2}$ N $_{1/2}$ , and BaSc $_{0.05}$ Ta $_{0.95}$ O $_{2.1}$ N $_{0.9}$ . J. Solid State Chem. **2007**, 180, 3224–3233.
- (40) Günther, E.; Hagenmayer, R.; Jansen, M. Strukturuntersuchungen an den Oxidnitriden SrTaO<sub>2</sub>N, CaTaO<sub>2</sub>N und LaTaON<sub>2</sub> mittels Neutronen- und Röntgenbeugung. *Z. Anorg. Allg. Chem.* **2000**, *626*, 1519–1525.
- (41) Yoshida, M.; Takanabe, K.; Maeda, K.; Ishikawa, A.; Kubota, J.; Sakata, Y.; Ikezawa, Y.; Domen, K. Role and Function of Noble-Metal/Cr-Layer Core/Shell Structure Cocatalysts for Photocatalytic Overall Water Splitting Studied by Model Electrodes. *J. Phys. Chem. C* **2009**, *113*, 10151–10157.
- (42) Goga, M.; Seshadri, R.; Ksenofontov, V.; Gütlich, P.; Tremel, W.  $Ln_2Ti_2S_2O_5$  (Ln = Nd, Pr, Sm): A Novel Series of Defective Ruddlesden–Popper Phases. *Chem. Commun.* **1999**, 979–980.

- (43) Ishikawa, A.; Takata, T.; Kondo, J. N.; Hara, M.; Kobayashi, H.; Domen, K. Oxysulfide Sm<sub>2</sub>Ti<sub>2</sub>S<sub>2</sub>O<sub>5</sub> as a Stable Photocatalyst for Water Oxidation and Reduction under Visible Light Irradiation ( $\lambda \leq$ 650 nm). J. Am. Chem. Soc. 2002, 124, 13547-13553.
- (44) Nishioka, S.; Kanazawa, T.; Shibata, K.; Tsujimoto, Y.; zur Loye, H.-C.; Maeda, K. A Zinc-Based Oxysulfide Photocatalyst SrZn<sub>2</sub>S<sub>2</sub>O Capable of Reducing and Oxidizing Water. Dalton Trans. 2019, 48, 15778-15781.
- (45) Zhang, G.; Wang, X. Oxysulfide Semiconductors for Photocatalytic Overall Water Splitting with Visible Light. Angew. Chem., Int. Ed. 2019, 58, 15580-15582.
- (46) Ishikawa, A.; Yamada, Y.; Takata, T.; Kondo, J. N.; Hara, M.; Kobayashi, H.; Domen, K. Novel Synthesis and Photocatalytic Activity of Oxysulfide Sm<sub>2</sub>Ti<sub>2</sub>S<sub>2</sub>O<sub>5</sub>. Chem. Mater. 2003, 15, 4442-4446.
- (47) Wang, Q.; Nakabayashi, M.; Hisatomi, T.; Sun, S.; Akiyama, S.; Wang, Z.; Pan, Z.; Xiao, X.; Watanabe, T.; Yamada, T.; Shibata, N.; Takata, T.; Domen, K. Oxysulfide Photocatalyst for Visible-Light-Driven Overall Water Splitting. Nat. Mater. 2019, 18, 827-832.
- (48) Huang, W. L.; Zhu, Q. Electronic Structures of Relaxed BiOX (X = F, Cl, Br, I) Photocatalysts. Comput. Mater. Sci. 2008, 43, 1101-
- (49) Li, J.; Yu, Y.; Zhang, L. Bismuth Oxyhalide Nanomaterials: Layered Structures Meet Photocatalysis. Nanoscale 2014, 6, 8473-
- (50) Di, J.; Xia, J.; Li, H.; Guo, S.; Dai, S. Bismuth Oxyhalide Layered Materials for Energy and Environmental Applications. Nano Energy 2017, 41, 172-192.
- (51) Li, J.; Li, H.; Zhan, G.; Zhang, L. Solar Water Splitting and Nitrogen Fixation with Layered Bismuth Oxyhalides. Acc. Chem. Res. 2017, 50, 112-121.
- (52) Xiong, J.; Song, P.; Di, J.; Li, H. Bismuth-Rich Bismuth Oxyhalides: A New Opportunity to Trigger High-Efficiency Photocatalysis. J. Mater. Chem. A 2020, 8, 21434-21454.
- (53) Wei, X.; Akbar, M. U.; Raza, A.; Li, G. A Review on Bismuth Oxyhalide Based Materials for Photocatalysis. Nanoscale Advances **2021**, *3*, 3353–3372.
- (54) Cheng, H.; Huang, B.; Dai, Y. Engineering BiOX (X = Cl, Br, I) Nanostructures for Highly Efficient Photocatalytic Applications. Nanoscale 2014, 6, 2009-2026.
- (55) Gordon, M. N.; Chatterjee, K.; Lambright, A. L.; Bueno, S. L. A.; Skrabalak, S. E. Organohalide Precursors for the Continuous Production of Photocatalytic Bismuth Oxyhalide Nanoplates. Inorg. Chem. 2021, 60, 4218-4225.
- (56) Ganose, A. M.; Cuff, M.; Butler, K. T.; Walsh, A.; Scanlon, D. O. Interplay of Orbital and Relativistic Effects in Bismuth Oxyhalides: BiOF, BiOCl, BiOBr, and BiOI. Chem. Mater. 2016, 28, 1980-1984.
- (57) Li, J.; Zhang, L.; Li, Y.; Yu, Y. Synthesis and Internal Electric Field Dependent Photoreactivity of Bi<sub>3</sub>O<sub>4</sub>Cl Single-Crystalline Nanosheets with High {001} Facet Exposure Percentages. Nanoscale 2014, 6, 167-171.
- (58) Lou, Z.; Wang, P.; Huang, B.; Dai, Y.; Qin, X.; Zhang, X.; Wang, Z.; Liu, Y. Enhancing Charge Separation in Photocatalysts with Internal Polar Electric Fields. ChemPhotoChem. 2017, 1, 136-147.
- (59) Li, M.; Huang, H.; Yu, S.; Tian, N.; Zhang, Y. Facet, Junction and Electric Field Engineering of Bismuth-Based Materials for Photocatalysis. ChemCatChem 2018, 10, 4477-4496.
- (60) Guo, Y.; Shi, W.; Zhu, Y. Internal Electric Field Engineering for Steering Photogenerated Charge Separation and Enhancing Photoactivity. EcoMat 2019, 1, No. e12007.
- (61) Sakthivel, T.; Venugopal, G.; Durairaj, A.; Vasanthkumar, S.; Huang, X. Utilization of the Internal Electric Field in Semiconductor Photocatalysis: A Short Review. J. Ind. Eng. Chem. (Amsterdam, Neth.) **2019**, 72, 18-30.
- (62) Kusainova, A. M.; Zhou, W.; Irvine, J. T. S.; Lightfoot, P. Layered Intergrowth Phases  $Bi_4MO_8X$  (X = Cl, M = Ta and X = Br, M = Ta or Nb): Structural and Electrophysical Characterization. J. Solid State Chem. 2002, 166, 148-157.

- (63) Fujito, H.; Kunioku, H.; Kato, D.; Suzuki, H.; Higashi, M.; Kageyama, H.; Abe, R. Layered Perovskite Oxychloride Bi<sub>4</sub>NbO<sub>8</sub>Cl: A Stable Visible Light Responsive Photocatalyst for Water Splitting. J. Am. Chem. Soc. 2016, 138, 2082-2085.
- (64) Bhat, S. S. M.; Swain, D.; Feygenson, M.; Neuefeind, J. C.; Mishra, A. K.; Hodala, J. L.; Narayana, C.; Shanbhag, G. V.; Sundaram, N. G. Bi<sub>4</sub>TaO<sub>8</sub>Cl Nano-Photocatalyst: Influence of Local, Average, and Band Structure. Inorg. Chem. 2017, 56, 5525-5536.
- (65) Tao, X.; Zhao, Y.; Mu, L.; Wang, S.; Li, R.; Li, C. Bismuth Tantalum Oxyhalogen: A Promising Candidate Photocatalyst for Solar Water Splitting. Adv. Energy Mater. 2018, 8, 1701392.
- (66) Chatterjee, K.; Banoo, M.; Mondal, S.; Sahoo, L.; Gautam, U. K. Synthesis of Bi<sub>3</sub>TaO<sub>7</sub>-Bi<sub>4</sub>TaO<sub>8</sub>Br Composites in Ambient Air and Their High Photocatalytic Activity upon Metal Loading. Dalton Trans. **2019**, 48, 7110-7116.
- (67) Ackerman, J. F. The Structures of Bi<sub>3</sub>PbWO<sub>8</sub>Cl and Bi<sub>4</sub>NbO<sub>8</sub>Cl and the Evolution of the Bipox Structure Series. J. Solid State Chem. 1986, 62, 92-104.
- (68) Zhou, X.; Dong, H. Density Functional Studies on Layered Perovskite Oxyhalide Bi<sub>4</sub>MO<sub>8</sub>X Photocatalysts (M = Nb and Ta, X = Cl, Br, and I). J. Phys. Chem. C 2017, 121, 20662-20672.
- (69) Payne, D. J.; Egdell, R. G.; Walsh, A.; Watson, G. W.; Guo, J.; Glans, P.-A.; Learmonth, T.; Smith, K. E. Electronic Origins of Structural Distortions in Post-Transition Metal Oxides: Experimental and Theoretical Evidence for a Revision of the Lone Pair Model. Phys. Rev. Lett. 2006, 96, 157403.
- (70) Walsh, A.; Payne, D. J.; Egdell, R. G.; Watson, G. W. Stereochemistry of Post-Transition Metal Oxides: Revision of the Classical Lone Pair Model. Chem. Soc. Rev. 2011, 40, 4455-4463.
- (71) Kato, D.; Hongo, K.; Maezono, R.; Higashi, M.; Kunioku, H.; Yabuuchi, M.; Suzuki, H.; Okajima, H.; Zhong, C.; Nakano, K.; Abe, R.; Kageyama, H. Valence Band Engineering of Layered Bismuth Oxyhalides toward Stable Visible-Light Water Splitting: Madelung Site Potential Analysis. J. Am. Chem. Soc. 2017, 139, 18725-18731.
- (72) Kunioku, H.; Higashi, M.; Tomita, O.; Yabuuchi, M.; Kato, D.; Fujito, H.; Kageyama, H.; Abe, R. Strong Hybridization between Bi-6s and O-2p Orbitals in Sillén–Aurivillius Perovskite  $Bi_4MO_8X$  (M = Nb, Ta; X = Cl, Br), Visible Light Photocatalysts Enabling Stable Water Oxidation. J. Mater. Chem. A 2018, 6, 3100-3107.
- (73) Suzuki, H.; Kunioku, H.; Higashi, M.; Tomita, O.; Kato, D.; Kageyama, H.; Abe, R. Lead Bismuth Oxyhalides PbBiO<sub>2</sub>X (X = Cl, Br) as Visible-Light-Responsive Photocatalysts for Water Oxidation: Role of Lone-Pair Electrons in Valence Band Engineering. Chem. Mater. 2018, 30, 5862-5869.
- (74) Ogawa, K.; Nakada, A.; Suzuki, H.; Tomita, O.; Higashi, M.; Saeki, A.; Kageyama, H.; Abe, R. Flux Synthesis of Layered Oxyhalide Bi<sub>4</sub>NbO<sub>8</sub>Cl Photocatalyst for Efficient Z-Scheme Water Splitting Under Visible Light. ACS Appl. Mater. Interfaces 2019, 11, 5642-5650.
- (75) Tao, X.; Shi, W.; Zeng, B.; Zhao, Y.; Ta, N.; Wang, S.; Adenle, A. A.; Li, R.; Li, C. Photoinduced Surface Activation of Semiconductor Photocatalysts under Reaction Conditions: A Commonly Overlooked Phenomenon in Photocatalysis. ACS Catal. 2020, 10, 5941-5948.
- (76) Kuriki, R.; Ichibha, T.; Hongo, K.; Lu, D.; Maezono, R.; Kageyama, H.; Ishitani, O.; Oka, K.; Maeda, K. A Stable, Narrow-Gap Oxyfluoride Photocatalyst for Visible-Light Hydrogen Evolution and Carbon Dioxide Reduction. J. Am. Chem. Soc. 2018, 140, 6648-6655.
- (77) Wakayama, H.; Utimula, K.; Ichibha, T.; Kuriki, R.; Hongo, K.; Maezono, R.; Oka, K.; Maeda, K. Light Absorption Properties and Electronic Band Structures of Lead Titanium Oxyfluoride Photocatalysts Pb<sub>2</sub>Ti<sub>4</sub>O<sub>9</sub>F<sub>2</sub> and Pb<sub>2</sub>Ti<sub>2</sub>O<sub>5.4</sub>F<sub>1.2</sub>. J. Phys. Chem. C 2018, 122, 26506-26511.
- (78) Hirayama, N.; Nakata, H.; Wakayama, H.; Nishioka, S.; Kanazawa, T.; Kamata, R.; Ebato, Y.; Kato, K.; Kumagai, H.; Yamakata, A.; Oka, K.; Maeda, K. Solar-Driven Photoelectrochemical Water Oxidation over an n-Type Lead-Titanium Oxyfluoride Anode. J. Am. Chem. Soc. 2019, 141, 17158-17165.

- (79) Chatterjee, K.; Dos Reis, R.; Harada, J. K.; Mathiesen, J. K.; Bueno, S. L. A.; Jensen, K. M. Ø.; Rondinelli, J. M.; Dravid, V.; Skrabalak, S. E. Durable Multimetal Oxychloride Intergrowths for Visible Light-Driven Water Splitting. *Chem. Mater.* **2021**, *33*, 347–358.
- (80) Chatterjee, K.; Bueno, S.; Skrabalak, S.; Dravid, V.; Reis, R. d. Nanoscale Investigation of Layered Oxychloride Intergrowth Photocatalysts for Visible Light Driven Water Splitting. *Microsc. Microanal.* **2020**, *26*, 376–379.
- (81) Nakada, A.; Kato, D.; Nelson, R.; Takahira, H.; Yabuuchi, M.; Higashi, M.; Suzuki, H.; Kirsanova, M.; Kakudou, N.; Tassel, C.; Yamamoto, T.; Brown, C. M.; Dronskowski, R.; Saeki, A.; Abakumov, A.; Kageyama, H.; Abe, R. Conduction Band Control of Oxyhalides with a Triple-Fluorite Layer for Visible Light Photocatalysis. *J. Am. Chem. Soc.* **2021**, *143*, 2491–2499.
- (82) Nakada, A.; Saeki, A.; Higashi, M.; Kageyama, H.; Abe, R. Two-Step Synthesis of Sillén—Aurivillius Type Oxychlorides to Enhance Their Photocatalytic Activity for Visible-Light-Induced Water Splitting. *J. Mater. Chem. A* **2018**, *6*, 10909—10917.
- (83) Tao, X.; Gao, Y.; Wang, S.; Wang, X.; Liu, Y.; Zhao, Y.; Fan, F.; Dupuis, M.; Li, R.; Li, C. Interfacial Charge Modulation: An Efficient Strategy for Boosting Spatial Charge Separation on Semiconductor Photocatalysts. *Adv. Energy Mater.* **2019**, *9*, 1803951.
- (84) Ozaki, D.; Suzuki, H.; Ogawa, K.; Sakamoto, R.; Inaguma, Y.; Nakashima, K.; Tomita, O.; Kageyama, H.; Abe, R. Synthesis, Band Structure and Photocatalytic Properties of Sillén—Aurivillius Oxychlorides BaBi<sub>5</sub>Ti<sub>3</sub>O<sub>14</sub>Cl, Ba<sub>2</sub>Bi<sub>5</sub>Ti<sub>4</sub>O<sub>17</sub>Cl and Ba<sub>3</sub>Bi<sub>5</sub>Ti<sub>5</sub>O<sub>20</sub>Cl with Triple-, Quadruple- and Quintuple-Perovskite Layers. *J. Mater. Chem. A* **2021**, *9*, 8332–8340.